2020 IEEE/RSJ International Conference on Intelligent Robots and Systems (IROS)
October 25-29, 2020, Las Vegas, NV, USA (Virtual)

Towards Micro Robot Hydrobatics: Vision-based Guidance, Navigation, and Control for Agile Underwater Vehicles in Confined Environments

Daniel A Duecker, Nathalie Bauschmann, Tim Hansen, Edwin Kreuzer, and Robert Seifried

***Abstract*— Despite the recent progress, guidance, navigation, and control (GNC) are largely unsolved for agile micro autonomous underwater vehicles (μAUVs). Hereby, robust and accurate self-localization systems which fit μAUVs play a key role and their absence constitutes a severe bottleneck in micro underwater robotics research. In this work we present, first, a small-size low-cost high performance vision-based self-localization module which solves this bottleneck even for the requirements of highly agile robot platforms. Second, we present its integration into a powerful GNC-framework which allows the deployment of μAUVs in fully autonomous mission. Finally, we critically evaluate the performance of the localization system and the GNC-framework in two experimental scenarios.**

I. Introduction

Hydrobatics refers to agile maneuvering of underactuated underwater vehicles and has become the marine counterpart of acrobatics in aerial robotics [1], [2], see Fig. 1. Agile underwater robots enable – beside the control design challenge – a wide range of applications such as monitoring of confined areas of interest e. g. aquaculture farms and harbors. These challenging tasks require robust and accurate control and localization strategies. Recent technological advances in robot miniaturization pushed this concept one step further resulting in the development of micro autonomous underwater vehicles (μAUVs) which are characterized by length scales of less than 50 cm. These small-scale systems allow deployment in monitoring missions within strictly confined volumes such as industry tanks and cluttered disaster sides e. g. the Fukushima-Daiichi reactor [3] which cannot be done using full-scale robots. Moreover, since μAUV designs usually aim for low-cost vehicles, deployment of underwater robot fleets becomes feasible and is expected to show the full capabilities of autonomously operating vehicles.

However, various bottlenecks hinder the development and deployment of μAUVs, namely embedded robust self-localization and powerful guidance, navigation, and control (GNC) architectures. While full and medium-scale underwater robot can be equipped with sophisticated sensing equipment such as ring-laser gyroscopes their deployment on μAUVs is infeasible due to their size and cost. Thus, a trade-off arises between miniaturization and autonomous capabilities.

This research was supported by the German Research Foundation (DFG) under grant Kr752/36-1.

All authors are with Hamburg University of Technology, Germany. Please direct correspondence to daniel.duecker@tuhh.de

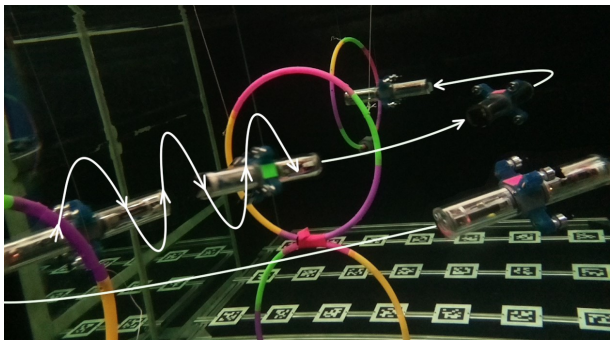

Fig. 1: Fully autonomous hydrobatic maneuvering through hoops gates with the HippoCampus μAUV.

Apparently, much work has been done on designing powerful control strategies for aerial robots [4]. Hence, transferring these concepts to the underwater domain is appealing. However, early-stage testing of these control algorithms even in controlled environments such as in research tanks remains challenging. It is often hindered due to the lack of robust and accurate on-board localization schemes which fit agile μAUVs.

A. Prior Work

Current research on μAUVs can be split into two approaches. Vehicles which are temporarily tethered can outsource major shares of the localization and control processing to an external computing unit which enables them to run complex algorithms. Recent work on these vehicles has shown great steps forward. Robust model predictive control in the presence of currents was presented in [5] while [6] demonstrated trajectory tracking under model uncertainties. However, due to their tether these vehicles can be seen as semi-autonomous, as the tether limits their freedom in path and motion planning especially in obstacle rich domains.

In contrast, tether-free vehicles are fully autonomous but have to rely on their on-board hardware. Literature [2], [7]–[9] shows a clear trade-off between a small vehicle size which offers a wide range of mission scenarios while it limits the capabilities of on-board sensors and computational power. An example for these restrictions is the non-availability of high-fidelity sensors in μAUVs such as ring-laser gyroscopes which are essential for dead reckoning based navigation as it is widely used in medium and full-size AUVs [10], [11].

978-1-7281-6211-9/20/$31.00 ©2020 IEEE

In contrast, state estimation systems based on small-size MEMS-sensors are widely used on μAUV platforms. Examples include the AVEXIS [7], the AUVx [8], and the HippoCampus [2], [9] underwater robots. However, due to the strong drift of dead reckoning when using MEMS-IMU data, μAUV navigation requires additional robust and continuous information on the vehicle's absolute position.

Accurate and robust on-board self-localization of μAUVs is required for fully autonomous operation. Moreover, modular concepts of on-board localization systems allow a quick replacement depending on in which scenario the robot is deployed.

External motion capture systems have been used to provide an accurate localization and even control commands to the underwater robot [12]–[15]. However, they require an underwater communication link to the robot which suffers from high latencies and a limited bandwidth and, thus, their usage is restricted to limited scenarios. Moreover, external systems do not scale with increasing vehicle fleet size. Hence, both aspects result in a bottleneck for research targeting agile control of underwater vehicles. In this sense, robust and accurate underwater localization in confined environments can still be seen as widely unsolved.

Localization systems and their challenges can be grouped following their physical principle into vision, acoustics, and electro-magnetic (EM) waves [16].

Vision based approaches use cameras to perceive the robot's environment. They aim to estimate the robot pose relative to detected features [17]. With regard to underwater applications their usage is mostly limited to short range detection and to clear water scenarios, as they require good visibility conditions. Artificial landmarks are a widely used concept in localization, as they can be used to enrich featureless environments such as halls and tanks. However, they require the effort of pre-mission deployment. This makes their usage attractive for controlled environments such as research testbeds. Classic approaches are based on illuminated markers and require the detection of a marker pattern to compute the robot's pose. Recently, powerful libraries such as the AprilTag marker system [18], [19] became available and are by now a standard method in robotics for pose estimation. The markers are uniquely distinguishable and come with the advantage of simultaneously providing information on position and orientation relative to the camera [10]. Studies on the robustness of fiducial marker detection in various water conditions were extensively conducted in [20] and demonstrated the general suitability for underwater applications, e. g. for insertion tasks [21]. Moreover, simultaneous localization and mapping (SLAM) techniques based on artificial markers were recently applied in underwater domains and have shown promising results [11], [22]. However, known concepts mainly cover comparatively slow motions as these are dominant in docking and manipulation tasks. Their extension to hydrobatic maneuvering, which is a common requirement in μAUV missions, remains an open field of research.

Self-localization systems based on acoustics are widely used for AUVs in open-sea scenarios. They typically use the signal's time-of-flight or time-difference-of-arrival to compute the vehicle's position relative to the sound signal emitting beacons. Recent work on small size acoustic modems made this technology available for μAUVs [23], [24]. While acceptable performance has been demonstrated in harbors and large tanks, missions which require precise positioning such as docking or trajectory tracking in e. g small research tanks remain out of today's capabilities. This is due to the fact that acoustic methods suffer massively from reflections caused by e. g. tank walls, reverberations, and multi-path effects [25].

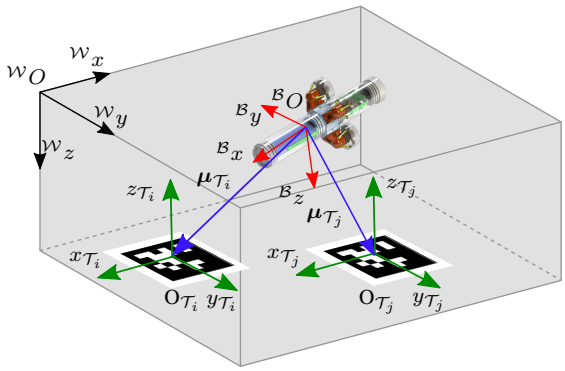

Fig. 2: μAUV navigating through a confined volume using AprilTag-based self-localization for feedback control.

The use of attenuation of electro-magnetic (EM) carrier waves for accurate short-range underwater localization was recently proposed in [26], [27]. This concept seems to be promising for confined volumes. The concept was miniaturized in [28] to fit the demands of μAUVs with respect to size and cost. Experiments using EM-localization for μAUV control in a small research tank have been conducted and analyzed in [29]. The tests demonstrated the general feasibility but also revealed the method's sensitivity to EM-wave reflections from the tank walls which limits deployment scenarios.

In summary, each concept comes with its specific advantages and disadvantages. However, when studying control strategies for fully autonomous hydrobatic maneuvering, existing approaches reach their limits. This is in particular the case for small-scale robotic systems. Thus, a bottleneck exists even for the potential simple scenario of testing the robot's autonomous capabilities in controlled environments such as research tanks.

B. Contribution

The contribution of this work is three-fold. First, we present an embedded, robust, and accurate visual localization system for μAUVs which enables agile trajectory tracking and path following in strictly confined volumes such as industry and research tanks. Moreover, our localization system can be used as temporary benchmark system for existing localization systems in the absence of external ground truth. Second, we propose a fully integrated GNC-framework and its combination with the developed self-localization concept.

Both the localization system and the GNC-module consists of low-cost off-the-shelf components (<USD 80 + Flight Control Unit USD 100) are open-source available under [1]. Their small size and open ROS-interface allow an easy integration on basically any micro underwater robot platform. Third, we provide experimental performance statistics on the single localization module in experiments. Additionally, we experimentally demonstrate the suitability of the integrated GNC-framework for agile feedback control in an hydrobatic path following scenario.

To the best of the author's knowledge there is no such system described in literature which provides μAUVs with the demonstrated amount of fully autonomous hydrobatic maneuvering capabilities.

The remainder of this work is structured as follows. Section II introduces the problem of self-localization for feedback control in agile maneuvering. The embedded localization module is described in Section III. Its integration into the GNC-framework is presented in Section IV. Experimental results are presented and critically discussed in Section V. Section VI summarizes the findings of this work and gives an outlook on future work.

II. Problem Statement

Consider the performance examination of the guidance, navigation and control architecture onboard a highly agile μAUV inside confined volumes such as small research tanks, as depicted in Fig. 1 and 2. The efficient development of sophisticated planning and control algorithms for μAUVs which allow the execution of complex fully autonomous missions is still hindered by today's absence of robust, accurate, and easy-to-use embedded localization modules which provide high-rate updates on the vehicle position and its yaw-orientation.

This capability gap is specific to the research on μAUVs, since full-scale AUVs and remotely operated vehicles (ROVs) can generally compensate this lack by using high-fidelity inertial measurement units [10], [11] or having access to powerful off-board computational capacities [5], [22]. Both approaches cannot be adapted to the domain of μAUVs as they are contrary to the goals of low-cost, small-size, and full autonomy.

We solve this problem by proposing a powerful visual fiducial marked-based localization module which fits the requirements of μAUVs such as size and energy consumption. Moreover, we embed the localization system into fully integrated GNC-framework as it is required for complex missions. Our proposed module features an open ROS-interface which makes it straight-forward to adapt to other μAUV platforms. In alignment with the idea of pushing forward marine robotics research through open-source concepts we make our module with all algorithms available online.

[1] https://github.com/DanielDuecker/microAUV-localization

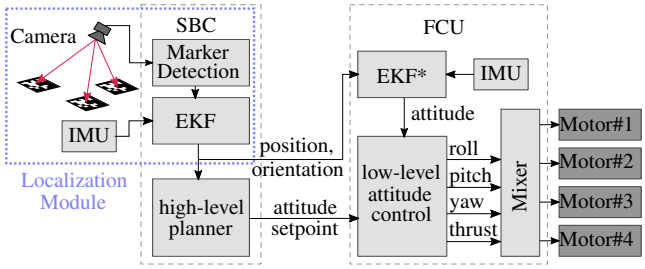

Fig. 3: Localization module embedded into the architecture of the GNC-framework. Algorithms on the SBC run at ∼10 Hz, Algorithms on the FCU run at ∼50 Hz.

III. Localization-Concept

In this work, we follow the idea of a platform independent localization system which can easily be adapted to the individual use-case. Thus, we aim to improve on general metrics such as high robustness and accuracy rather than overfitting to scenario specific requirements.

The developed localization module consists of three on-board components, namely a camera, an inertial measurement unit (IMU), and a single board computer (SBC), as depicted in Fig. 3. However, in order to deploy the system the target volume, e. g. the research tank, has to be equipped with fiducial markers at known positions. While various marker systems exist we select – without loss of generality – the AprilTag system [19].

An on-board wide-angle camera collects images of the vehicle's surrounding environment. A detection algorithm [30] extracts AprilTags from the image and computes their position and orientation relative to the camera. This information is then fed into a sensor fusion algorithm which fuses the measured tags' position and orientation and provides uncertainty measures on both. In order to provide high-frequent updates on the robot state, e. g. for controllers, we require inter-observations predictions steps. Note that our estimation algorithm focuses on the most challenging robot states in underwater robotics, namely the robot's position and the yaw-orientation.

Robust yaw measurements of the yaw-angle e. g. using on-board magnetometers is often infeasible. In practice, strong magnetic disturbances lead to severe local deviations of the magnetic field which is a common challenge in small (steel) tanks and render the magnetometer-based yaw-signal intractable for most navigation tasks.

In this work, we propose an extended Kalman Filter (EKF) scheme which we extend by a dynamic measurement noise model. Note that the basic version of this filter is commonly used in the robotics community. Thus, adaptions to individual scenarios remain straight-forward. However, the choice of other sensor fusion algorithms, such as particle filtering, is of course possible.

Let ${}^{\mathcal{W}}\boldsymbol{x}_k$ be the position and orientation of the robot's body frame $\mathcal{B}$ in a world-fixed coordinate system $\mathcal{W}$ at time k

$$ {}^{\mathcal{W}}\boldsymbol{x}_k = \left[x, y, z, \phi, \theta, \psi\right]^\top, \tag{1} $$

where x, y, z are the vehicle position and the angles roll ϕ, pitch θ, and yaw ψ represent its orientation $\boldsymbol{\Theta}$, respectively.

The robot dynamics are approximated by a simple velocity model $\boldsymbol{f}$ following Fossen [31] which is supplemented by the translational accelerations measured by the on-board IMU. Complex motion models can be incorporated to improve the filter's prediction accuracy. However, they require a model parameter identification which is specific to the individual vehicle on which the localization module is deployed [32].

The AprilTag detection algorithm provides accurate distance information $d_{\mathcal{T}_i}$ between the body frame $\mathcal{B}$ and the i-th detected AprilTag marker $\mathcal{T}_i$. However, the AprilTag-measured orientations in roll and pitch direction show an unreliable jumpy behavior for various robot orientations which is not acceptable for localization in agile maneuvering scenarios. Since computing the pitch and roll orientation from IMU data is robust, we restrict our AprilTag-based estimate to position and yaw-orientation ψ. Thus, the estimated state at time step k reduces to $\hat{\boldsymbol{p}}(k) = [x, y, z, \psi]^\top$.

The state update is based on the measurement $\boldsymbol{\mu}$ which is modeled by the nonlinear observation function $\boldsymbol{h}(\boldsymbol{p})$. It consists of the distances $d_{\mathcal{T}_i}$ between the robot and the detected AprilTags $\mathcal{T}_i$ which are located at known positions and orientation inside the tank. The single tag-distance measurement yields

$$\mu_i = h_i(\boldsymbol{p}) = \sqrt{\left({}^{\mathcal{W}}\boldsymbol{p} - {}^{\mathcal{W}}O_{\mathcal{T}_i}\right)^2}, \tag{2}$$

where ${}^{\mathcal{W}}O_{\mathcal{T}_i}$ is the known position of the i-th tag. Thus, the measurement vector $\boldsymbol{\mu}$ capturing N detected markers yields

$$\boldsymbol{\mu}_k = \left[\boldsymbol{\mu}_{k\mathcal{T}_1} \cdots \boldsymbol{\mu}_{k\mathcal{T}_N}\right] \tag{3}$$

with

$$\boldsymbol{\mu}_{k\mathcal{T}_i} = \left[d_{k\mathcal{T}_i}\ \psi_{k\mathcal{T}_i}\right]^\top. \tag{4}$$

Note that the dimension of μ changes dynamically with the number of markers detected N in every camera frame.

Thus, the corresponding Jacobian matrix has the form

$$\boldsymbol{J}_{\boldsymbol{p}(k)} = \left[\nabla_{\boldsymbol{p}(k)} h_1(\boldsymbol{p}(k))^\top \cdots \nabla_{\boldsymbol{p}(k)} h_N(\boldsymbol{p}(k))^\top\right]^\top. \tag{5}$$

The predicted state and its covariance read

$$\hat{\boldsymbol{p}}^{(-)}(k) = \boldsymbol{f}\left(\hat{\boldsymbol{p}}^{(+)}(k-1)\right) \quad \text{and} \tag{6}$$

$$\hat{\boldsymbol{P}}^{(-)}(k) = \hat{\boldsymbol{P}}^{(+)}(k-1) + \boldsymbol{Q}, \tag{7}$$

where $\boldsymbol{Q}$ represents the corresponding process noise matrix in diagonal form. The superscripts (-) and (+) indicate values gained before and after incorporating the measurement μ respectively.

In order to update the estimated state based on the measurement $\boldsymbol{\mu}$ the Kalman-gain reads

$$\boldsymbol{K}(k) = \hat{\boldsymbol{P}}^{(-)}(k)\boldsymbol{J}_{\boldsymbol{p}(k)}\left(\boldsymbol{J}_{\boldsymbol{p}(k)}\hat{\boldsymbol{P}}^{(-)}(k)\boldsymbol{J}_{\boldsymbol{p}(k)}^\top + \boldsymbol{R}\left(\boldsymbol{q}^{\mathcal{C}}\right)\right)^{-1} \tag{8}$$

where $\boldsymbol{R}(\boldsymbol{q}^{\mathcal{C}})$ is the measurement noise. Note that we use dynamic measurement noise in order to incorporate the uncertainties which origin from the camera fish-eye lens,

$$\boldsymbol{R}(\boldsymbol{q}) = \|\boldsymbol{q}^{\mathcal{C}}\| / \left(\boldsymbol{q}^{\mathcal{C}} \boldsymbol{e}_3^{\mathcal{C}} c_{\text{penalty}}\right), \tag{9}$$

where $\boldsymbol{q}^{\mathcal{C}}$ the measured tag-position in x-y-z-camera coordinates, $\boldsymbol{e}_3^{\mathcal{C}}$ is the $z^{\mathcal{C}}$-axis unit vector of the camera frame, and c_{penalty} is a tuning parameter. Equation 9 dynamically increases the measurement noise $\boldsymbol{R}$ for individual tag measurements which appear on the border of the camera's field of view. These measurements are usually affected by distortions in the image rectification process which we capture by higher measurement noise. This can be seen as a soft outlier penality and considerably increases localization robustness during dynamic maneuvers when many tags appear at the field of view border, e. g the roll screw maneuver depicted in Fig. 1 and discussed in Sec. V-B.

Thus, the state update yields

$$\hat{\boldsymbol{p}}^{(+)}(k) = \hat{\boldsymbol{p}}^{(-)}(k) + \boldsymbol{K}(k)\left(\boldsymbol{\mu}(k) - \boldsymbol{h}(\hat{\boldsymbol{p}}^{(-)}(k))\right), \tag{10}$$

$$\hat{\boldsymbol{P}}^{(+)}(k) = \left(\boldsymbol{I} - \boldsymbol{K}(k)\boldsymbol{J}_{\boldsymbol{p}(k)}\right)\hat{\boldsymbol{P}}^{(-)}(k). \tag{11}$$

Note that we compensate for individual time stamp shifts. However, this requires to run the filter algorithm on a delayed fusion horizon. The compensation of this delay which is required for agile control method is described in the following section.

IV. GNC-Framework

A. Architecture

In the following, we embed the localization module into a fully integrated GNC-framework, depicted in Fig. 3. Beside the previously developed localization module, the GNC-framework possesses a high-level planning module which breaks down the mission task into robot attitude setpoints. These are processed by a low-level attitude controller which computes the corresponding control commands. The control signals are fed into a mixing module which maps the signals onto the individual motor actuators. This mapping step is based on the geometric actuator configuration of the robot and, thus, allows a simple adaptation of the GNC-framework towards other robot platforms. With respect to the hardware, we group the software modules into algorithms running on the SBC at a low update rate, e. g. the planner, and high-rate modules such as the low-level attitude controller which are implement on the flight computing unit (FCU). Both computing units exchange data via a high bandwidth serial MAVROS-interface.

In order to preserve the modular concept, we follow a loosely coupled estimation approach. Note that the localization data can be subject to non-negligible latencies mainly due to image processing. These latencies have to be compensated in order to achieve optimal data quality for agile maneuvering control. Since the low-level control algorithms are running on board the PX4-based FCU [33], a time-delay compensation can hardly capture potential latencies on the SBC-FCU-communication within the SBC-based

localization module. Thus, we integrate the data stream from the localization module into PX4's estimation framework (EKF* in Fig. 3) which is optimized to handle individual sensor latencies. It consists of an EKF which is running on a delayed fusion time horizon and a complementary filter which propagates the state to the current time.

B. Planning and Control-Design

In order to achieve high modularity we propose a hierarchical planning and control design consisting of two layers: First, a high-level planning algorithm computes attitude setpoints in order to follow a given trajectory or path. Second, a low-level attitude controller which computes the required motor commands based on the robot's current attitude $\boldsymbol{\Theta}$ and the given attitude setpoints $\boldsymbol{\Theta}_{\mathrm{des}}$. In order to compute target attitude setpoints for the low-level controller, we plan cubic path segments from the robot's current pose towards the target path. This is found an efficient strategy and leads to improved results in comparison to a standard pure pursuit algorithm [31]. However, more sophisticated planning strategies are of course possible.

In this work, we exemplary consider the control problem of the underactuated HippoCampus μAUV platform [2]. While four degrees of freedom can be actuated directly, sway and heave remain unactuated. Note that the modular architecture of the proposed GNC-module allows for a flexible adaptation to a wide variety of other underwater robot platforms. The control output $\boldsymbol{u}$ represents the thrust u_1 in the robot's ${}^{\mathcal{B}}x$-axis direction of as well as the moments u_2, u_3, and u_4 around the ${}^{\mathcal{B}}x$, ${}^{\mathcal{B}}y$, and ${}^{\mathcal{B}}z$-axis respectively

$$\boldsymbol{u} = \begin{bmatrix} u_1 & 0 & 0 & u_2 & u_3 & u_4 \end{bmatrix}^{\top}. \tag{12}$$

We propose a low-level PD-controller based on the control scheme presented by Mellinger et al. [34] which is originally designed for aggressive aerial drone maneuvering. However, its application in underwater robotics is so far limited to robust attitude stabilization [2]. For the sake of simplicity we assume the thrust signal u_1 to a constant target value $u_{1,\mathrm{des}}$ while the outputs u_2 to u_4 are computed as follows. Let the vector $\boldsymbol{e}_{\mathrm{R}}$ describe the robot's orientation error with regard to the desired orientation $\boldsymbol{R}_{\mathrm{des}} = \boldsymbol{R}(\boldsymbol{\Theta}_{\mathrm{des}})$

$$\boldsymbol{e}_{\mathrm{R}} = \begin{bmatrix} e_{\mathrm{R}^{\mathcal{B}}\mathrm{x}} \\ e_{\mathrm{R}^{\mathcal{B}}\mathrm{y}} \\ e_{\mathrm{R}^{\mathcal{B}}\mathrm{z}} \end{bmatrix} = \frac{1}{2}\left(\boldsymbol{R}_{\mathrm{des}}^{\top}\boldsymbol{R}(\Theta) - \boldsymbol{R}(\boldsymbol{\Theta})^{\top}\boldsymbol{R}_{\mathrm{des}}\right)^{\vee}, \tag{13}$$

where $^{\vee}$ is the *vee map* operator which is used for the transformation from $SO(3)$ to $\mathbb{R}^3$. Note that for the case of large orientation errors, we temporary reduce u_1 to prioritize the minimization of the orientation error. Moreover, we define the error of the corresponding angular velocities as

$$\boldsymbol{e}_{\omega} = \boldsymbol{\omega} - \boldsymbol{\omega}_{\mathrm{des}}. \tag{14}$$

Thus, the resulting control outputs yield

$$\begin{bmatrix} u_2 & u_3 & u_4 \end{bmatrix}^{\top} = -\boldsymbol{K}_{\mathrm{R}}\boldsymbol{e}_{\mathrm{R}} - \boldsymbol{K}_{\omega}\boldsymbol{e}_{\omega}, \tag{15}$$

where $\boldsymbol{K}_{\mathrm{R}}$ and $\boldsymbol{K}_{\omega}$ are diagonal matrices which allow convenient gain tuning of the individual components.

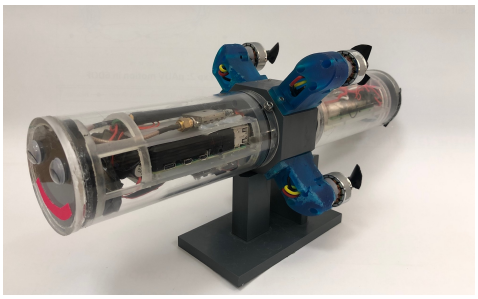

Fig. 4: Modular μAUV platform HippoCampus, length 40 cm, hull diameter 7 cm, with front-mounted GNC-module.

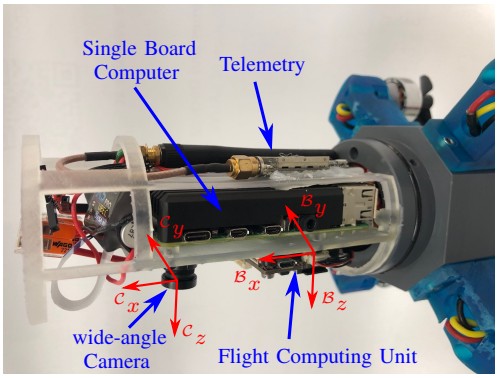

Fig. 5: GNC-system including the localization module mounted on the μAUV platform HippoCampus.

C. Hardware Design

The μAUV localization module mainly consists of three components, depicted in Fig. 5: a wide-angle camera, an SBC and a FCU. The camera is a low-cost wide-angle RaspberryPi camera with an opening angle of 140°. Note that the effective opening angle is approximately 120° due to rectification. We reduce the resolution to 640×480 px in order to trade-off accuracy against processing time which allows the vision-system to run at 10 Hz. Note that other camera mounting orientations are possible to adapt the system to the individual robot design. A Raspberry Pi 4 with 4 Gb RAM is chosen as an on-board SBC running the vision processing and the EKF. The PixRacer-platform is used as an FCU running the PX4-firmware [33] including a dedicated μAUV attitude controller. This modular design allows to physically split the low-frequent components e. g. the vision processing from the high-frequent components such as the attitude controller. Figure 5 shows the complete module in a 3D-printed rack which fits the dimensions of the HippoCampus μAUV, see Fig 4. However, all system components fit into a total volume of approximately $90 \times 50 \times 30$ mm. The system is powered with 5 V and its power consumption is 9 W at full load which is comparatively low in comparison to the high power consumption of the four thrusters. For more details on the HippoCampus platform we refer the reader to [2], [35].

V. Experiments

We evaluate the performance of our system in two experimental settings. First, we analyze the accuracy of the proposed embedded visual localization system. In a second

experiment, we analyze the GNC-framework in combination with the localization module. Hereby, the goal is to drive the system to its limits by driving hydrobatic maneuvers fully autonomously.

The experiments are conducted within a $4 \times 2 \times 2\,\mathrm{m}$ fresh water tank. The tank is equipped with an array of 63 AprilTags with $400 \times 250\,\mathrm{mm}$ spacing. Note that we use coarser configurations out of the mounted 63 tag-array for the individual experiments. We choose the AprilTag-family 36h11 with side-lengths of 9.6 cm. Early testing shows that this tag size can be detected at 3 m using low-cost RaspberryPi camera at $640 \times 480\,\mathrm{px}$ which makes the use of AprilTags attractive also for larger tanks. Further distances are possible when using a higher resolution. For all experiments the localization module is deployed on board the HippoCampus μAUV, see Fig. 4 and 5. The acryl tube hull has a wall thickness of 3 mm. Prior to the experiments, we calibrate the wide-angle camera underwater using standard checkerboard calibration. We refer the reader to the accompanying video for an intuitive visual understanding.

A. Localization Performance

In the following we analyze the performance of the proposed localization module in order to demonstrate its suitability for accurate visual underwater localization and benchmarking tasks. Prior works, such as [20], focus their analysis of the AprilTag detection mainly on static or slow-motion settings with high-performance camera equipment. Therefore, our analysis supplements these prior results by a *dynamic* tracking setup. In order to benchmark our results against ground truth data, we mount the localization module onto an automated gantry system which can follow desired paths with in x-y-z-direction with millimeter accuracy. In order to analyze whether the localization accuracy drops in certain areas of the tank volume we conduct the experiment at three different depths levels which represent varying distances d between the localization module and the tag-array. Moreover, we examine three tag-array densities, namely the a *fine* array with 31 tags, a *coarse* setup with only 23 tags, and the full array with *all* 63 AprilTags as a baseline.

The results for all configurations are summarized in Tab. I. The cross track error e_{cross} is defined between the gantry's path and the estimated position and, thus, independent from latencies e. g. due to processing time and time stamp shifts. Moreover, the results show that for larger distances the tag-density has only a small influence on the localization accuracy. However, in the 0.4 m setup, the coarse array leads to an observable accuracy drop as only few tags appear in the cameras field of view.

Figure 6 shows the position estimate exemplary for the experimental setup with distance $d = 0.8\,\mathrm{m}$ and the dense-array. It can be seen that the module consistently achieves high accuracy throughout the tank volume (RMSE $e_{\mathrm{cross}} = 2.6\,\mathrm{cm}$). The accuracy drops slightly in areas close to the tank walls (see x≈0 m and x≈3.1 m) due to the reduced number of visible AprilTags in the camera's field of view. Moreover, the camera can be subject to motion blur which can considerable reduce the number of detected tags. Therefore, we examine this effect in more detail in Sec. V-B. Note that the algorithm only detects markers which completely lie within its field of view. The analysis of the raw camera images shows that often multiple AprilTags lie only partly in the field of view which can result in a reduced accuracy. Thus, a trade-off arises between long and short detection distances, using large and small markers, respectively. Moreover, we can observe that even tags visible in acute angles from the camera can be detected robustly as long as they lie within the field of view.

TABLE I: Cross-track error e_{cross} of the position estimated and the average number of AprilTags n_{tags} detected at each camera frame for various camera to tag-array distances d. The corresponding standard deviations are denoted in parentheses. The setup with gray background is depicted in detail in Fig. 6.

Dist.	d	1.3 m	0.8 m	0.4 m
all	e_{cross}	3.1 (1.2) cm	2.4 (0.7) cm	3.8 (5.3) cm
	n_{tags}	23.1 (4.7)	12.3 (3.1)	4.2 (2.2)
fine	e_{cross}	3.1 (1.4) cm	2.6 (1.3) cm	5.5 (4.4) cm
	n_{tags}	11.6 (2.3)	6.1 (1.6)	1.8 (0.8)
coarse	e_{cross}	3.4 (1.8) cm	3.2 (1.6) cm	14.9 (20.5) cm
	n_{tags}	8.6 (1.7)	4.8 (1.3)	1.7 (1.1)

As expected, the average number of detected tags has a strong effect on the localization performance. Especially larger tanks allow a coarse tag distribution which still ensures that enough tags lie in the camera's field of view. However, the mounting of the tags can be adjusted depending on the task.

Finally, we examine the localization module's capability of estimating its yaw orientation with respect to the marker array. This is an important aspect for μAUVs since determining the robot's yaw orientation is usually strongly effected by distortions of the magnetic field leading to inaccurate measurements of the magnetometers. Therefore, we move the localization module along straight lines through the tank with its own orientation fixed. This allows to determine the deviation of the yaw estimate during the motion. We conduct multiple experimental runs with different fixed orientations of the localization module. The resulting standard deviation remains by less than 2° which can be seen as a drastic improvement in comparison to standard magnetic field based concepts which often render infeasible in confined tanks consisting of steel frames.

In summary, the experiment demonstrates the high accuracy of the localization module. Note that the above reported results are achieved with low-cost components of less than USD 80.

B. Hydrobatic Path Tracking Control

Our second experiment focuses on the robustness of the localization system and its integration into the GNC-framework. In order to demonstrate the performance of the system, we design a challenging sequence of hydrobatic maneuvers. The sequence consists of an ∞-shape path at varying depths and a screw-maneuver, where the robot turns

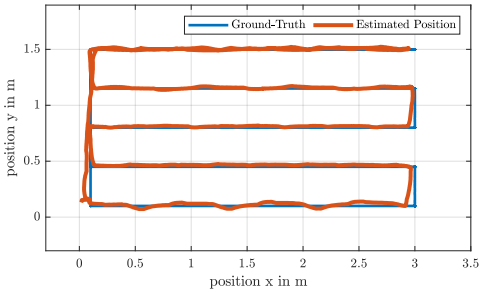

Fig. 6: Accuracy of the localization module in comparison to ground truth.

360° around its roll-axis while following the path, see Fig. 1. The outer dimensions of the path are $2.5 \times 0.9\,\mathrm{m}$ with a total length of 4.4 m. As no external tracking system is available we place fixed hoops as gates with 50 cm diameter as reference points on the robot's path to the visualize the path containing envelope, see Figs. 1 and 7.

The path is processed on board the SBC by the high-level planning module with a 35 cm planning horizon. The recorded track is depicted in Fig. 7 for four consecutive rounds at varying depths. Note that we pose an additional challenge to the system at the beginning of the experiment by throwing the robot through the air to an arbitrary starting position. The localization system recovers within the first few time instances and estimates the correct position, see the accompanying video.

When driving hydrobatic maneuvers, accurate and robust information on the current robot position are required. Therefore, we want to point out the tracking performance during the screw-maneuver when the system cannot see and detect any marker for 2.7 s. For this time span the controller relies purely on the EKF prediction. Note that, after regaining visual contact to the tags no noticeable jumps are induced by the Kalman update. Figure 8 shows the number of detected markers while following the path for one round, including the zero sight segment in dark red which corresponds to the screw maneuver. The reader is referred to the accompanying video to get a more intuitive understanding of the maneuvering sequence. When examining the raw camera images, it can be seen that the camera greatly suffers from motion blur when the vehicle is performing agile maneuvers. However, tuning the camera exposure time can reduce this effect. We refer the reader to the *rosbag*-files which were recorded during the experiments which are linked to code-repository.

It is worth mentioning that the robot is able to track the path at all time instances with small cross-track errors (RMSE 7.2 cm). Thereby, it follows the μAUV is able to follow at significant higher speed than similar state of the art autonomous underwater robot platforms. During the experiment, the angular velocities reach up to $[4, 2.8, 1.5]$ rad/s for roll, pitch, and yaw rotations, respectively.

As a result, although we pose several challenges, the experiments demonstrate that our proposed GNC-framework is capable to repeatably and accurately drive the μAUV along the path.

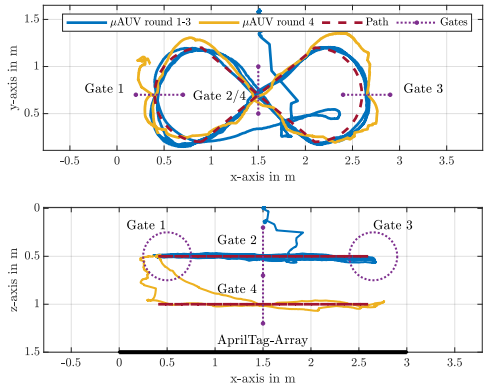

Fig. 7: Tracking performance of the HippoCampus μAUV driving through four hoop gates.

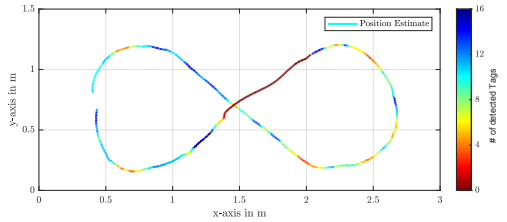

Fig. 8: Number of detected AprilTags during the first ∞-round. The red segment indicates zero tag-detections during the screw maneuver, see also Fig. 1

VI. Conclusion

A. Summary

In this work, we propose a robust high accuracy marker-based visual self-localization system in combination with a guidance, navigation, and control (GNC) architecture which allow hydrobatic maneuvering with agile micro underwater robots. The developed concept provides small-scale submerged robots with reliable information on their absolute position and orientation, as well as the corresponding control commands by only using low-cost components.

The developed concept forms an independent localization module which can be used as either a primary source of position information or as a secondary system for benchmarking purposes. We demonstrate in two experiments, first, the strong robustness and accuracy of the self-localization module on its own and, second, the capability of the integrated GNC-system of driving an agile micro underwater robot along a path while performing hydrobatic maneuvers. Herewith, we overcome one of the major bottlenecks in micro underwater robotics research, as experiments on fully autonomous missions were challenging even in controlled environments such as research tanks. Our algorithms are available online under `https://github.com/DanielDuecker/microAUV-localization`. The algorithms and findings in the evaluations are likely contributing to other researchers' work in micro underwater robotics, as the adaptation of our system to other platforms is straight-forward.

B. Future Work

The proposed self-localization system in combination with the GNC-framework opens several directions of future research. Since it provides robust and accurate information in the robot's absolute position, the framework is expected to accelerate development of more sophisticated trajectory planning and following algorithms. With regard to μAUV navigation, we will investigate the effect of additional cameras and varying AprilTag-setups on the localization performance.

REFERENCES

[1] S. Bhat and I. Stenius, "Hydrobatics: A Review of Trends, Challenges and Opportunities for Efficient and Agile Underactuated AUVs," in *AUV 2018 - 2018 IEEE/OES Autonomous Underwater Vehicle Workshop, Proceedings*. Porto: IEEE, 2018, pp. 1–8.

[2] D. A. Duecker, A. Hackbarth, T. Johannink, E. Kreuzer, and E. Solowjow, "Micro Underwater Vehicle Hydrobatics: A Submerged Furuta Pendulum," in *IEEE International Conference on Robotics and Automation (ICRA)*. Brisbane: IEEE, 2018, pp. 7498–7503.

[3] M. Nancekievill, A. R. Jones, M. J. Joyce, B. Lennox, S. Watson, J. Katakura, K. Okumura, S. Kamada, M. Katoh, and K. Nishimura, "Development of a Radiological Characterization Submersible ROV for Use at Fukushima Daiichi," *IEEE Transactions on Nuclear Science*, vol. 65, no. 9, pp. 2565–2572, 2018.

[4] F. Kendoul, "Survey of Advances in Guidance, Navigation, and Control of Unmanned Rotorcraft Systems," *Journal of Field Robotics*, vol. 29, no. 2, pp. 315–378, 2012.

[5] S. Heshmati-Alamdari, G. C. Karras, P. Marantos, and K. J. Kyriakopoulos, "A Robust Model Predictive Control Approach for Autonomous Underwater Vehicles Operating in a Constrained workspace," in *2018 IEEE International Conference on Robotics and Automation (ICRA)*. Brisbane: IEEE, 2018, pp. 6183–6188.

[6] C. P. Bechlioulis, G. C. Karras, S. Heshmati-Alamdari, and K. J. Kyriakopoulos, "Trajectory Tracking With Prescribed Performance for Underactuated Underwater Vehicles Under Model Uncertainties and External Disturbances," *IEEE Transactions on Control Systems Technology*, vol. 25, no. 2, pp. 429–440, 2017.

[7] A. Griffiths, A. Dikarev, P. R. Green, B. Lennox, X. Poteau, and S. Watson, "AVEXIS - Aqua vehicle explorer for in-situ sensing," *IEEE Robotics and Automation Letters*, vol. 1, no. 1, pp. 282–287, 2016.

[8] H. Hanff, P. Kloss, B. Wehbe, P. Kampmann, S. Kroffke, A. Sander, M. B. Firvida, M. V. Einem, J. F. Bode, and F. Kirchner, "AUVx - A Novel Miniaturized Autonomous Underwater Vehicle," in *Oceans*. Aberdeen: IEEE, 2017, pp. 1–10.

[9] A. Hackbarth, E. Kreuzer, and E. Solowjow, "HippoCampus: A micro underwater vehicle for swarm applications," in *IEEE/RSJ International Conference on Intelligent Robots and Systems (IROS)*. Hamburg: IEEE, 9 2015, pp. 2258–2263.

[10] J. Jung, J. H. Li, H. T. Choi, and H. Myung, "Localization of AUVs using visual information of underwater structures and artificial landmarks," *Intelligent Service Robotics*, vol. 10, no. 1, pp. 67–76, 2017.

[11] J. Jung, Y. Lee, D. Kim, D. Lee, H. Myung, and H.-t. Choi, "AUV SLAM Using Forward / Downward Looking Cameras and Artificial Landmarks," *IEEE Underwater Technology (UT)*, pp. 1–3, 2017.

[12] D. J. Klein, P. K. Bettale, B. Triplett, and K. A. Morgansen, "Autonomous underwater multivehicle control with limited communication: Theory and experiment," *Proceedings of the 2008 IFAC Workshop on Navigation, Guidance and Control of Underwater Vehicles*, vol. 41, no. 1, pp. 113–118, 2008.

[13] S. Napora and D. A. Paley, "Observer-Based Feedback Control for Stabilization of Collective Motion," *IEEE Transactions on Control Systems Technology*, vol. 21, no. 5, pp. 1846–1857, 9 2013.

[14] N. Sydney, S. Napora, S. Beal, P. Mohl, P. Nolan, S. Sherman, A. Leishman, S. Butail, and D. A. Paley, "A Micro-UUV Testbed for Bio-Inspired Motion Coordination," *Int. Symp. Unmanned Untethered Submersible Technology*, pp. 1–13, 2009.

[15] R. Cui, Y. Li, and W. Yan, "Mutual Information-Based Multi-AUV Path Planning for Scalar Field Sampling Using Multidimensional RRT*," *IEEE Transactions on Systems, Man, and Cybernetics: Systems*, vol. 46, no. 7, pp. 993–1004, 2016.

[16] A. Dikarev, A. Griffiths, S. A. Watson, B. Lennox, and P. R. Green, "Combined multiuser acoustic communication and localisation system for microAUVs operating in confined underwater environments," *IFAC Workshop on Navigation, Guidance and Control of Underwater Vehicles*, vol. 48, no. 2, pp. 161–166, 2015.

[17] M. Ishida and K. Shimonomura, "Marker Based Camera Pose Estimation for Underwater Robots," in *IEEE/SICE International Symposium on System Integration*. Fukuoka: IEEE/SICE, 2012, pp. 629–634.

[18] E. Olson, "AprilTag : A robust and flexible visual fiducial system," in *IEEE International Conference on Robotics and Automation (ICRA)*. Shanghai: IEEE, 2011, pp. 3400–3407.

[19] J. Wang and E. Olson, "AprilTag 2 : Efficient and robust fiducial detection," in *IEEE/RSJ International Conference on Intelligent Robots and Systems*. Deajeon: IEEE/RSJ, 2016, pp. 2–7.

[20] D. B. dos Santos Cesar, C. Gaudig, M. Fritsche, M. A. dos Reis, and F. Kirchner, "An Evaluation of Artificial Fiducial Markers in Underwater Environments," in *IEEE OCEANS*, Genova, 2015, pp. 1–6.

[21] E. H. Henriksen, I. Schjølberg, and T. B. Gjersvik, "Vision Based Localization for Subsea Intervention," in *Proceedings of the ASME 2017 36th International Conference on Offshore Mechanics and Arctic Engineering (OMAE)*, Trondheim, 2017, pp. 1–9.

[22] E. Westman and M. Kaess, "Underwater AprilTag SLAM and calibration for high precision robot localization," Carnegie Mellon University, Pittsburgh, PA, Tech. Rep. October, 2018.

[23] J. Heitmann, F. Steinmetz, and C. Renner, "Self-Localization of Micro AUVs Using a Low-Power , Low-Cost Acoustic Modem," in *OCEANS 2018 MTS/IEEE*. Charleston: IEEE, 2018, pp. 72–74.

[24] Q. Tao, Y. Zhou, F. Tong, A. Song, and F. Zhang, "Evaluating acoustic communication performance of micro autonomous underwater vehicles in confined spaces," *Frontiers of Information Thechnology and Electronic Engineering*, vol. 19, no. 8, pp. 1013–1023, 2018.

[25] A. R. Geist, A. Hackbarth, E. Kreuzer, V. Rausch, M. Sankur, and E. Solowjow, "Towards a hyperbolic acoustic one-way localization system for underwater swarm robotics," in *Proceedings - IEEE International Conference on Robotics and Automation (ICRA)*, Stockholm, 2016, pp. 4551–4556.

[26] D. Park, K. Kwak, J. Kim, and W. K. Chung, "3D Underwater Localization Scheme using EM Wave Attenuation with a Depth Sensor," in *IEEE International Conference on Robotics and Automation (ICRA), 2016*. Stockholm: IEEE, 2016, pp. 2631–2636.

[27] D. Park, J. Jung, K. Kwak, J. Kim, and W. K. Chung, "Received Signal Strength of Electromagnetic Waves Aided Integrated Inertial Navigation System for Underwater Vehicle," in *IEEE/RSJ International Conference on Intelligent Robots and Systems*, IEEE, Ed., Madrid, 2018, pp. 1870–1876.

[28] D. A. Duecker, A. R. Geist, M. Hengeler, E. Kreuzer, M. A. Pick, V. Rausch, and E. Solowjow, "Embedded spherical localization for micro underwater vehicles based on attenuation of electro-magnetic carrier signals," *Sensors (Switzerland)*, vol. 17, no. 5, 2017.

[29] D. A. Duecker, T. Johannink, E. Kreuzer, V. Rausch, and E. Solowjow, "An Integrated Approach to Navigation and Control in Micro Underwater Robotics," in *(accepted to) IEEE International Conference on Robotics and Automation (ICRA)*. Montreal: IEEE, 2019, pp. 1–7.

[30] D. Malyuta, C. Brommer, D. Hentzen, T. Stastny, R. Siegwart, and R. Brockers, "Long-duration fully autonomous operation of rotorcraft unmanned aerial systems for remote-sensing data acquisition," *Journal of Field Robotics*, vol. August, pp. 1–21, 2019.

[31] T. I. Fossen, *Handbook of Marine Craft Hydrodynamics and Motion Control*. Wiley, 2011.

[32] D. A. Duecker, E. Kreuzer, G. Maerker, and E. Solowjow, "Parameter Identification for Micro Underwater Vehicles," in *Proceedings in Applied Mathematics and Mechanics (PAMM)*, no. June. Munich: GAMM, 2018, pp. 1–2.

[33] L. Meier, D. Honegger, and M. Pollefeys, "PX4: A node-based multithreaded open source robotics framework for deeply embedded platforms," in *2015 IEEE International Conference on Robotics and Automation (ICRA)*. Seattle: IEEE, 5 2015, pp. 6235–6240.

[34] D. Mellinger and V. Kumar, "Minimum Snap Trajectory Generation and Control for Quadrotors," in *IEEE International Conference on Robotics and Automation (ICRA)*. Shanghai: IEEE, 2011, pp. 2520–2525.

[35] D. Duecker, E. Solowjow, and A. Hackbarth, "The open-source HippoCampus Robotics Project," 2020. [Online]. Available: https://hippocampusrobotics.github.io/